Inorganic Chemistry Communications 170 (2024) 113348

Contents lists available at ScienceDirect

Inorganic Chemistry Communications

journal homepage: www.elsevier.com/locate/inoche

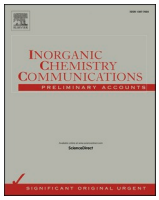

Short communication

Dynamics of Lanthanide(III) complexes from crystallographic data and computational studies

Charlene Harriswangler [a], Saray Argibay-Otero [a,b], Antía Freire-García [a], M. Teresa Albelda [c], Enrique García-España [c,d], David Esteban-Gómez [a], Juan C. Frías [e,*], Carlos Platas-Iglesias [a,*]

[a] Universidade da Coruña, Centro de Interdisciplinar de Química e Bioloxía (CICA) and Departamento de Química, Facultade de Ciencias, 15071, A Coruña, Galicia, Spain
[b] Departamento de Química Inorgánica, Universidade de Vigo, Facultad de Ciencias, 36310 Vigo, Spain
[c] Departamento de Química Inorgánica, Universidad de Valencia, 46100 Burjasot, Valencia, Spain
[d] Instituto de Ciencia Molecular (ICMol), Departamento de Química Inorgánica, Universidad de Valencia, 46980 Paterna, Spain
[e] Departamento de Ciencias Biomédicas, Universidad Cardenal Herrera-CEU, CEU Universities, 46115 Alfara del Patriarca, Spain

ARTICLE INFO

Keywords:
Lanthanides
Polyaminocarboxylates
Dynamics
DFT
Rare-earths
Macrocycles
Force constants

ABSTRACT

In this study we take advantage of the large body of X-ray data reported for lanthanide complexes, as well as their similar coordination chemistry properties, to gain insight on the dynamic processes involving λ ↔ δ configurational changes leading to isomer interconversion. The analysis of X-ray data reveals that different donor groups are characterized by Gaussian distributions of the dihedral N–C–X–Y angles ϕ. In the case of ethylenediamine groups (X = C; Y = N) Gaussian distributions are very narrow, while acetates (X = C; Y = O) provide very broad distributions. The analysis of the potential energy surfaces (PESs) using DFT reveals that ethylenediamine groups are characterised by well-defined deep energy minima, while those of acetate groups are rather swallow. Other donor groups like acetamide, pyridine or phosphinate show intermediate Gaussian distributions with respect to ethylenediamine and acetates. The PESs were fitted to a potential incorporating quadratic, cubic and quartic terms. The quadratic force constants k_{11} obtained for the different donor types follow the trend of the full width at half maxima (FWHM) of Gaussian distributions obtained from X-ray data. The k_{11} values are very similar for a given donor group, while the anharmonic cubic (k_{111}) and quartic (k_{1111}) force constants vary significantly depending on the environment of the donor group. Overall, this work demonstrates that the analysis of X-ray crystallographic data in lanthanide complexes can provide very useful information on their coordination chemistry preferences and dynamic processes.

1. Introduction

The coordination chemistry of lanthanide(III) ions in aqueous media has been the subject of intense research efforts over the past four decades [1–6]. Early works reported in the early 1960 s evidenced that DTPA forms very stable complexes with the Ln(III) ions [7], exceeding the stability of EDTA analogues by several orders of magnitude [8,9]. Two decades later it was discovered that the macrocyclic ligand DOTA forms very stable and inert complexes with the lanthanides [10–15]. Since then, DOTA and DTPA were considered the gold standards for lanthanide complexation, with the macrocyclic structure of DOTA resulting in slow complexation and dissociation kinetics, in sharp contrast to DTPA derivatives (Scheme 1) [16,17]. The Gd(III) complexes with these ligands and closely related derivatives were introduced as

Abbreviations: H_4AAZTA, 6-amino-6-methylperhydro-1,4-diazepinetetraacetic acid; CSD, Cambridge structural database; DFT, Density Functional Theory; H_3DO3A = 1, 4,7,10-tetrazacyclononane-1,4,7-triacetic acid; H_4DOTA, 1,4,7,10-tetraazacyclododecane-1,4,7,10-tetraacetic acid; DOTAM, 1,4,7,10-tetrakis(carbamoylmethyl)-1,4,7,10-tetraazacyclododecane; H_4DOTP^H, ((1,4,7,10-tetraazacyclododecane-1,4,7,10-tetrayl)tetrakis(methylene))tetrakis(phosphinic acid); H_5DTPA, diethylenetriamine-*N*,*N*,*N*′,*N*″,*N*″-pentaacetic acid; H_3DTPA-BMA, 1,7-bis[(*N*-methylcarbamoyl)methyl]-1,4,7-triazaheptane-1,4,7-triacetic acid; H_4EDTA = ethylenediamine-*N*, *N*,*N*′,*N*′-tetraacetic acid; H_4EGTA, ethylene glycol-bis(2-aminoethylether)-*N*,*N*,*N*′,*N*′-tetraacetic acid; FWHM, full width at half maxima; IEF-PCM, Integral equation formalism polarized continuum model; MRI, Magnetic Resonance Imaging; H_4OBETA, 2,2′,2″,2‴-((oxybis(ethane-2,1-diyl))bis(azanetriyl))tetraacetic acid; PES, potential energy surface.

* Corresponding authors.
E-mail addresses: juan.frias@uchceu.es (J.C. Frías), carlos.platas.iglesias@udc.es (C. Platas-Iglesias).

https://doi.org/10.1016/j.inoche.2024.113348
Received 1 August 2024; Received in revised form 1 October 2024; Accepted 16 October 2024
Available online 20 October 2024

contrast agents for magnetic resonance imaging (MRI) in the late 1980 s and 1990 s [18,19]. The development of MRI contrast agents based on these scaffolds continued over the years [20], with a tetrameric Gd(III) DOTA derivative currently being in advanced clinical trials [21]. Research efforts were also conducted to prepare Ln(III) complexes of DTPA and DOTA derivatives for other applications, including the design of luminescent probes [22–25] and radiopharmaceuticals [26–28].

The dynamics of Ln(III) complexes of DOTA and DTPA derivatives have been investigated rather extensively using NMR techniques, providing detailed information on the exchange of coordinated water molecules with the bulk [29], as well as the dynamic processes responsible for the interconversion between the different stereoisomers present in solution [30–33]. Computational studies were also very important to provide detailed information on these dynamic processes at the molecular level [34–37], an issue of great relevance to understand the efficiency of MRI contrast agents and their behavior in solution [38]. Isomer interconversion involves changes in configuration of five-membered chelate rings formed upon coordination of the ligand to the metal ion. The chelate rings formed upon coordination of the ethylenediamine and acetate units of DTPA and DOTA derivatives are not planar. The puckering of these chelate rings can be measured by the corresponding N–C–C–N and N–C–C–O dihedral angles, which may take positive or negative values, corresponding to the conformations referred as to δ and λ, respectively (Fig. 1). The interconversion between isomers present in solution involves δ ↔ λ interconversions of these chelate rings [1,32,36]. The puckering of five-membered chelate rings has been related with the dynamics of δ ↔ λ exchange in transition metal complexes [39]. Other dynamic processes that have been investigated in Ln(III) DOTA derivatives are the rotation of acetate arms, which exchanges the coordinated and un-coordinated oxygen atoms of acetate groups. This exchange process involves high activation energy barriers compared to the δ ↔ λ interconversion process in both Ln(III)-DOTA and Ln(III)-DTPA complexes [40–42].

In a recent work, we used the structures of DOTA and DTPA derivatives reported in the Cambridge Structural Database (CSD) to derive a series of donor radii that allow estimating Ln(III)-donor distances for any lanthanide cation regardless its coordination number and oxidation state.[43] Herein, we sought to use the same set of data to gain information on the dynamics of Ln(III) complexes by analyzing the dihedral angles characterizing the coordination of different structural motifs present in DTPA and DOTA derivatives. The information obtained from X-ray data was further analyzed using computational studies based on state of the art density function theory (DFT). The puckering of these dihedral angles provides valuable information on the structure and dynamics of Ln(III) complexes.

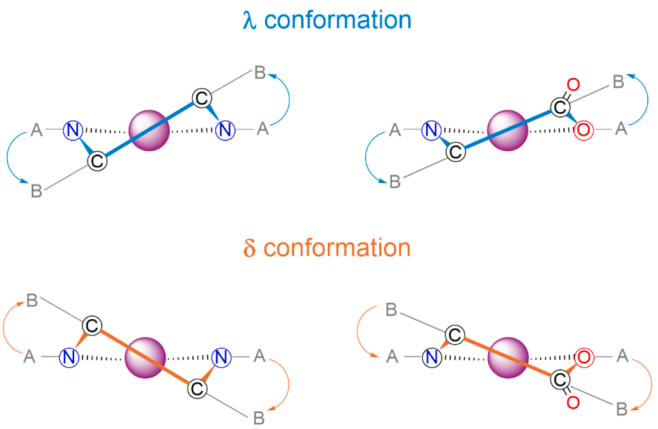

Fig. 1. Schematic representation of the δ and λ conformations of five-membered chelate rings formed by ethylenediamine (left) and acetate (right) groups.

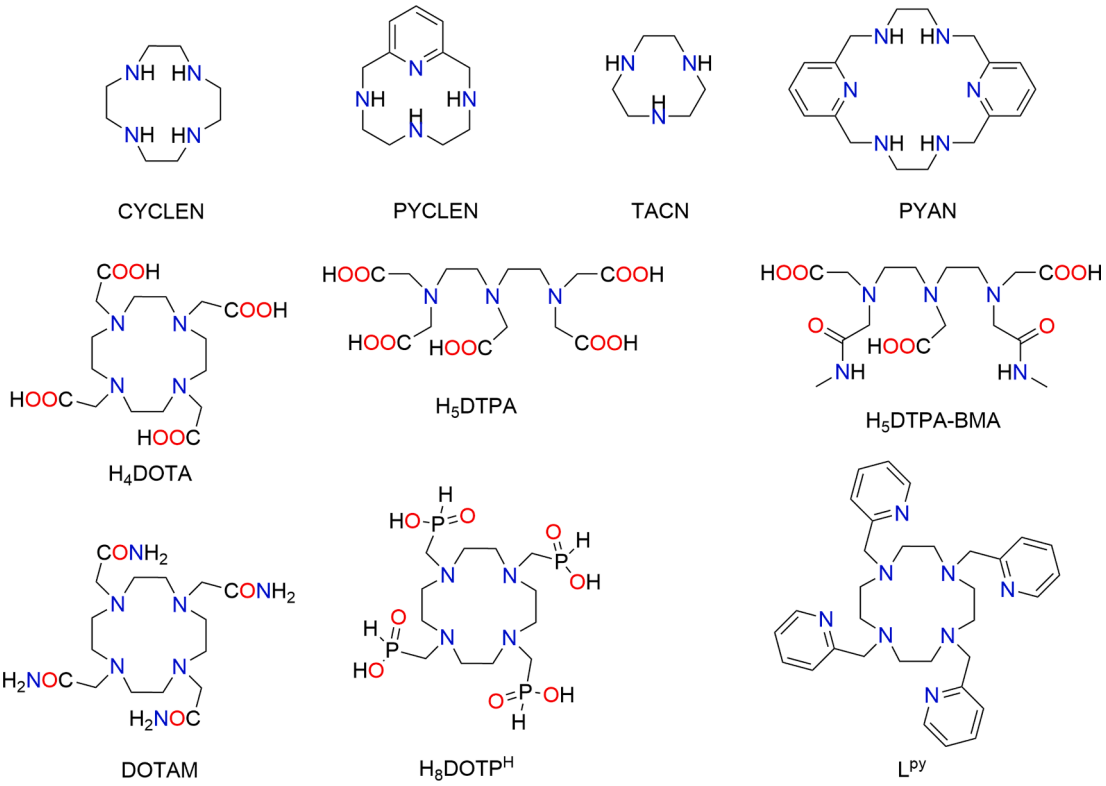

Scheme 1. Ligands discussed in this work.

2. Methods

2.1. CSD data

The crystal structures of rare-earth complexes of the DTPA and DOTA families were retrieved from the CSD after an extensive and careful search. A full list of the structures analyzed, their CSD codes and dihedral angles are provided in the Supplementary material (Tables S1-S16). A few structures have been reported in the Protein Data Bank (PDB) in which DOTA derivatives were co-crystallized with proteins. However, the different torsion angles measured in these macromolecular structures exhibit significant differences with respect to the small molecule crystals, and thus they were omitted in this work (see for instance Ref. [44]).

2.2. DFT calculations

The geometries of the Gd(III) complexes were optimized using Gaussian 16 [45], employing the range-separated hybrid wB97XD functional [46], which incorporates empirical dispersion corrections. This functional performs well to compute the geometries, energy barriers and coordination numbers of lanthanide complexes [47–49]. No explicit second-sphere water molecules were considered, in spite of being necessary to compute accurate Gd–O_{water} distances and ^{17}O spin densities [50,51]. However, inclusion of explicit second sphere water molecules also increases the complexity of the PES, by generating different local energy minima with similar energies. Relativistic effects were incorporated using the quasi-relativistic effective core potential ECP53MWB for Gd(III), which includes 46 + $4f^7$ electrons in the core, together with the associated (8s7p6d3f2g)/[6s5p5d3f2g] valence basis set (ECP53MWB-II) [52,53]. The standard Def2–TZVPP basis set was used for the ligand atoms [54]. Bulk water solvent effects were incorporated with the integral equation formalism variant of PCM (IEF-PCM variant) [55,56]. Frequency calculations confirmed that the optimized geometries corresponded to actual energy minima. The size of the integration grid was augmented with the integral = superfinegrid keyword. Relaxed potential energy surface scan were performed starting from the optimized geometries using the opt = modredundant option of Gaussian. Optimized Cartesian coordinates of the structures used in this work and a sample input file are provided in the Supplementary material (Tables S17-S23). Test calculations performed on the $Gd(NH_2)_3$ system show that the wB97XD/ECP53MWB/ Def2–TZVPP method provides a PES virtually identical to the gold standard coupled-cluster CCSD(T) method [57]. Additionally, calculations using a small core (wB97XD/ECP28MWB/Def2–TZVPP) indicate that the use of large (53 electrons) or small (28 electrons) cores provide very similar PESs [58] (Fig. S1).

3. Results and discussion

3.1. Puckering of five-membered chelate rings involving ethylenediamine, acetate and acetamide groups

The puckering of the five-membered chelate rings in lanthanide(III) complexes was analysed by using a dataset comprising the X-ray structures of all DTPA and DOTA derivatives deposited to date in the CSD (79 and 364 structures, respectively). Both these important families of complexes contain ethylenediamine units in their scaffolds that form five-membered chelate rings upon coordination to the metal ion. Some structural features of these chelate rings have been reviewed recently [59].

The N-C-C-N torsion angles characterising the ethylenediamine chelate rings have absolute values close to 60°, at an average of 59.3°. This is expected, as a value of 60° yields a staggered conformation of the ethyl groups [60]. No significant differences are observed in the distributions of ethylenediamine groups in DTPA and DOTA derivatives, for which the average values are 62.7 and 59.0°, respectively. As was stated in the introduction, the N–C–C–N dihedrals may take positive or negative values, corresponding to the conformations referred as to δ and λ, respectively [60]. Nevertheless, DTPA and DOTA complexes often crystallise as racemates, with two enantiomers being present in the crystal. Thus, the sign of the N-C-C-N torsion angles measured from crystal data does not necessary reflect the presence of one particular stereoisomer, but rather that selected to define the asymmetric unit. Nevertheless, the values of the N-C-C-N torsion angles in DOTA and DTPA complexes yield two quite symmetrical Gaussian distributions centred at ± 59.1° and a full width at half maximum (FWHM) of only ~ 6.3° (Fig. 2). We interpret this rather narrow distribution of the dihedral angles as the result of a deep energy minimum on the potential energy surface. This is in line with different NMR studies, which indicated a rather high free energy barrier for the δ ↔ λ interconversion of five-membered chelate rings in DTPA and DTPA-bisamide lanthanide complexes (~55 kJ/mol) [30,61]. The interconversion in DOTA derivatives were found to possess similar activation free energies [33].

The N-C-C-N torsion angles characterising the ethylenediamine chelate rings of complexes with macrocyclic derivatives of TACN, PYCLEN and PYAN were also analysed to assess the effect of macrocyclic ring size and rigidity. These macrocyclic platforms have found rather widespread use for stable lanthanide complexation [62–65]. We obtain mean values close to 60° for PYCLEN (59.4°, 58 values) and PYAN (58.0°, 42 values), in agreement with the distributions observed for DOTA and DTPA derivatives. However, TACN derivatives display broader distribution centered at 47.3 ± 0.1° (FWHM = 13.5°, 190 values), which is far away from the ideal value of 60° (Fig. S2). This indicates that the coordination of lanthanide ions to the small-sized TACN ring introduces a certain degree of strain to the macrocyclic unit, while the larger rings of CYCLEN, PYCLEN and PYAN can accommodate the metal ion while maintaining N-C-C-N torsion angles close to 60°.

The 1,4,7,10-tetraazacyclododecane framework was functionalized with a rather wide range of pendant arms, among which acetate and acetamide groups are the most common ones (i. e. in DOTA and DOTAM, respectively). A similar situation holds for DTPA derivatives. The N-C-C-O dihedrals of coordinated acetate groups show a very broad distribution, with absolute values in the range 0 – 45° and an average absolute value of 20.6°. DTPA and DOTA complexes are characterized by similar average absolute values of 18.6 and 21.8°, respectively. The histogram of N-C-C-O dihedrals display two maxima at + 21.0 ± 0.5° and −19.7 ± 0.5°, with FWHM values of 27.2° and 25.0°, respectively (Fig. 2, see also Table 1). The position of the maxima reflects the formation of less

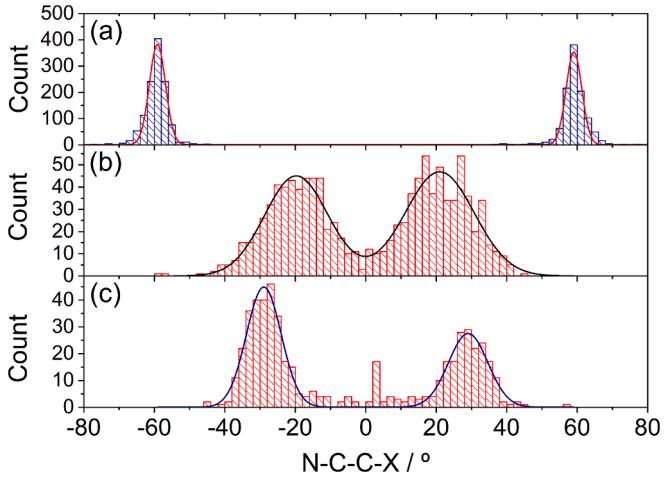

Fig. 2. Histograms showing the N-C-C-X dihedral angles characterizing five-membered chelate rings in DTPA and DOTA derivatives: (a) Ethylenediamine groups (X = N); (b) Acetate groups (X = O); (c) Acetamide groups (X = O). The solid lines correspond to the fits of the data to Gaussian distributions.

Table 1
Centre (x_c, °) and full width at half maximum (FWHM, °) of the Gaussian distributions of dihedral angles in lanthanide(III) complexes.[a].

Donor group	dihedral	x_c	FWHM
Ethylenediamine[b]	N-C-C-N	59.07 ± 0.07	6.2 ± 0.2
		−59.13 ± 0.06	6.4 ± 0.2
Acetate[b]	N-C-C-O	21.0 ± 0.5	27.2 ± 1.4
		−19.7 ± 0.5	25.0 ± 1.4
Acetamide[b]	N-C-C-O	29.1 ± 0.4	15.5 ± 1.2
		−28.9 ± 0.3	13.7 ± 0.7
Pyridine[c]	N-C-C-N	32.0 ± 0.2	7.4 ± 0.4
Phosphinate[c]	N-C-P-O	25.2 ± 0.2	11.7 ± 0.4

[a] Standard errors of the least-squares fits are also provided. [b] Dihedral angles fitted to a double Gaussian distribution. [c] Absolute values of dihedral angles fitted to a single Gaussian function.

puckered chelate rings compared with the ethylenediamine moieties. Furthermore, the very broad distribution of the two maxima suggests a rather low activation energy for the δ ↔ λ interconversion, which should proceed through a transition state in which the five-membered chelate ring is planar. In the case of an ethylenediamine chelate, this leads to an eclipsed conformation of the H atoms of the neighbouring C atoms. The absence of hydrogen atoms at the carbonyl C atom is likely responsible, at least in part, of the broad distribution of dihedral angles. This suggests that the δ ↔ λ interconversion associated to the rotation of acetate groups should be characterized by low activation energies, unless steric effects of vicinal groups hinder the process. This has been nicely demonstrated for [Ln(DOTA)]$^-$ complexes, in which the rotation of the four acetate arms follows a concerted process characterized by a rather large activation free energy (> 50 kJ/mol) [35]. However, the lack of a pendant arm in [Ln(DO3A)] complexes results in much lower energy barriers for the rotation of acetate arms (~20 kJ/mol) [66]. A fast δ ↔ λ interconversion of the acetate groups is also compatible with the NMR spectra reported for Ln(III) complexes of acyclic ligands such as EGTA and OBETA, as well as the mesocyclic AAZTA ligand [67–69].

A rather large number of X-ray structures of DOTA and DTPA amide derivatives have been reported (142 structures, see Supplementary material). The analysis of N-C-C-O dihedrals of acetamide groups evidences that their chelate rings are significantly more puckered than those involving acetates, with two slightly asymmetrical Gaussian distributions with maxima at 29.1 ± 0.4° and –28.9 ± 0.3°, and FWHM values of 15.5° and 13.7°, respectively (Fig. 2). Thus, Gaussian distributions are narrower for acetamides than for acetates, indicating that likely the δ ↔ λ interconversion in acetamides is associated to higher activation energies than for acetates. Of note, all DTPA and DOTA derivatives containing primary amide groups are *Z* isomers, and thus the NH amide group points to the methylenic CH_2 protons. The presence of the *E* isomer in solution was postulated recently on the bases of NMR data recorded for Eu(III)·DOTA-monoamide complexes containing chiral centers in both α or δ positions of the acetamide pendant arm [70].

The N-C-C-O dihedrals involving acetate and acetamide pendant arms do not correlate with the observed Ln–O bond distances. This can be clearly seen in Fig. 3, which plots the dihedral angles versus the Ln-O distance for Gd(III) complexes. Bond distances are obviously dependent not only on the particular Ln(III) ion, but also on the coordination number. However, the DOTA and DTPA Gd(III) derivatives considered here largely contain nine-coordinated metal ions (~95 %), with the remaining complexes having eight-coordinated Gd(III) ions. The plots shown in Fig. 3 display scattered haphazard points, demonstrating that there is no correlation between the Gd–O distances and the dihedral angles. The Ln–O distances involving acetate groups tend to be slightly shorter than those of acetamide groups.

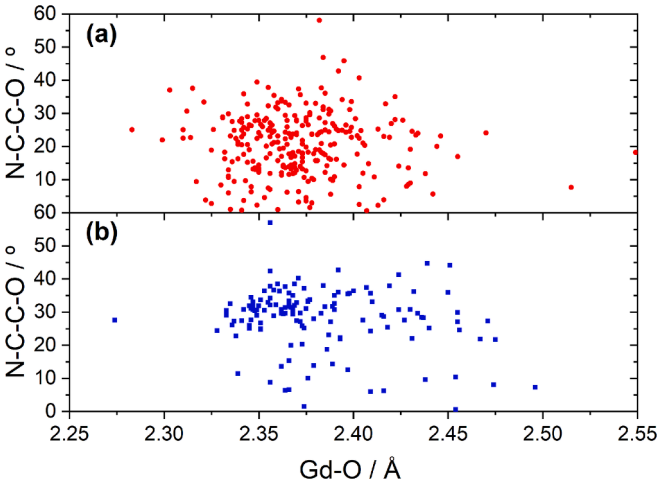

Fig. 3. Plots of the absolute values of N-C-C-O dihedral angles characterizing five-membered chelate rings in Gd(III) DTPA and DOTA derivatives versus the corresponding Gd-O bond distances: (a) acetate groups, (b) acetamide groups.

3.2. Potential energy surfaces of five-membered chelate rings involving ethylenediamine, acetate and acetamide groups

Relaxed potential energy surface (PES) scans were performed on the $[Gd(DTPA)(H_2O)]^{2-}$ and [Gd(DTPA-BMA)(H_2O)] complexes using DFT calculations (see computational details above). The potential energy surfaces obtained upon scanning the two N–C–C–N dihedral angles (ϕ) of ethylenediamine groups reveal rather deep energy minima at ~+65° (Fig. 4). The positive signs of the two dihedral angles indicates that these five-membered chelate rings adopt δ configurations. Conversely, the N–C–C–O dihedral angles of acetate groups are all negative, reflecting λ configurations of the corresponding chelate rings. The position of the minimum varies slightly depending on the specific acetate group, ranging from –22.0° to −26.6°. Thus, the position of the energy minima on the PESs of both ethylenediamine and acetate groups are close to the centres of their Gaussian distributions observed in the solid state (Table 1).

The signs of ϕ indicate that the optimized structure of the [Gd(DTPA)(H_2O)]$^{2-}$ complex displays a Λ(δδ) configuration, where Λ indicates the overall helicity originating from the layout of the five acetate pendant

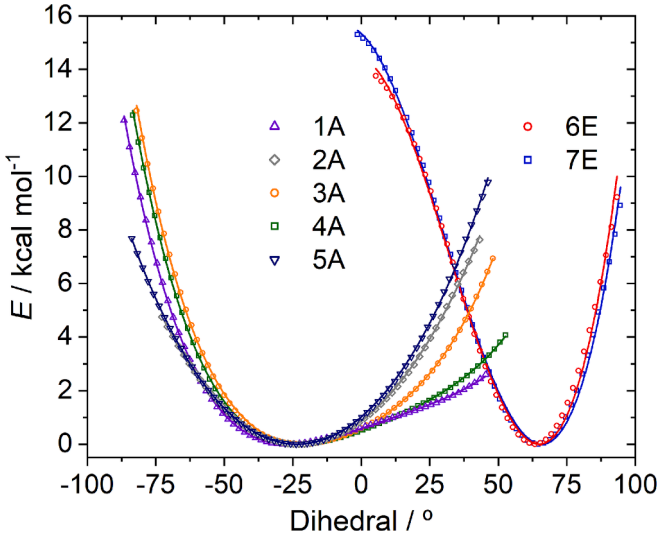

Fig. 4. Relaxed PESs obtained with DFT for acetate groups 1A-5A and ethylenediamine groups 6E and 7E in $[Gd(DTPA)(H_2O)]^{2-}$. The lines correspond to the fit of the data as explained in the text.

arms (Fig. 5). It is worth mentioning that the $[Gd(DTPA)(H_2O)]^{2-}$ complex has been crystallized in the form of the Ag^+, aminoguanidine, and K^+ salts, all of which display (δδ) configurations of the ethylenediamine groups [71–73]. While most of the acetate groups display λ configurations, some of them display dihedral angles close to zero or even positive. However, this is not surprising considering the curves shown in Fig. 4, which reveal that the N–C–C–O dihedrals of acetate groups define a rather swallow PES. The shape of the PESs generated for the five acetate groups is relatively similar on the negative side of dihedral angles, which imply bending the acetate group towards a neighbouring one. This provokes a steep increase in energy associated to steric and electrostatic repulsive effects arising from approximating two carboxylate groups. However, they differ considerably as the dihedral angle takes positive values. For instance, chelate rings 2A and 5A generate relatively symmetrical PESs. This indicates that the modification of the dihedral angle from the equilibrium value causes comparable energy penalties regardless the direction taken on the PES. This shape is in sharp contrast to those generated by chelate rings 1A and 4A. In the case of the latter, the dihedral N–C–C–O angle ϕ can vary from –23.4° up to 45° at an energy cost of only ~ 2 kcal mol^{-1}.

The PESs calculated with DFT can be represented in the vicinity of the energy minimum by a quadratic potential characterized by a force constant k_{11}. However, the analysis of the PESs over a wide range of ϕ values requires the introduction of anharmonic cubic and quartic terms, characterised by force constants k_{111} and k_{1111}, respectively:

$$E(\phi) = \frac{1}{2}k_{11}(\phi - \phi_e)^2 + \frac{1}{2}k_{111}(\phi - \phi_e)^3 + \frac{1}{2}k_{1111}(\phi - \phi_e)^4 \quad (1)$$

In Eq [1), ϕ represents the value of the dihedral angle and ϕ_e is the value of the dihedral at equilibrium [74]. The PESs calculated for both ethylenediamine and acetate groups can be fitted very well to Eq [1], affording the force constants and ϕ_e values presented in Table 2. Obviously, the quadratic and quartic terms can only have positive contributions to the energy, while the cubic term has opposite contributions at each side of ϕ_e (Fig. 6). Thus, high k_{11} and k_{1111} values contribute to steep the energy increase on both sides of ϕ_e, while a high k_{111} value has a positive contribution to energy on the negative side of ϕ_e and a negative contribution on the positive side. The quartic term has an increasing contribution with respect to the quadratic term as ϕ deviates from ϕ_e. Thus, the k_{1111} force constants likely catch steric and electrostatic interactions occurring within the molecule upon significant changes in ϕ, as the concern group approaches neighbouring molecule fragments.

The harmonic k_{11} force constants obtained for the five chelate rings are rather similar, being within the range (2.7–3.7) × 10^{-3} kcal mol^{-1} deg^{-2}. The corresponding values obtained for the ethylenediamine groups are ~ 6 times higher, in line with the deep energy minima of their PESs and the narrow distribution of ϕ values observed in X-ray data. The two ethylenediamine groups are characterized by similar anharmonic cubic force constants k_{111}. However, acetate groups show significant variations on their k_{111} values. In particular, chelate ring 2A is characterised by a k_{111} value being one order of magnitude smaller than those of acetate groups 1A and 4A. This indicates that chelate 2A has a rather harmonic PES that originates from important steric and electrostatic effects taking place as ϕ takes more positive values. Chelate ring 5A shows a similar behaviour, though to a lesser extent than 5A. Thus, the k_{111} values provide an estimate of the environmental effects that hinder the rotation of the acetate group as ϕ changes sign, with lower k_{111} values indicating more important steric and/or electrostatic effects that hinder acetate rotation. Nevertheless, both k_{111} and k_{1111} force

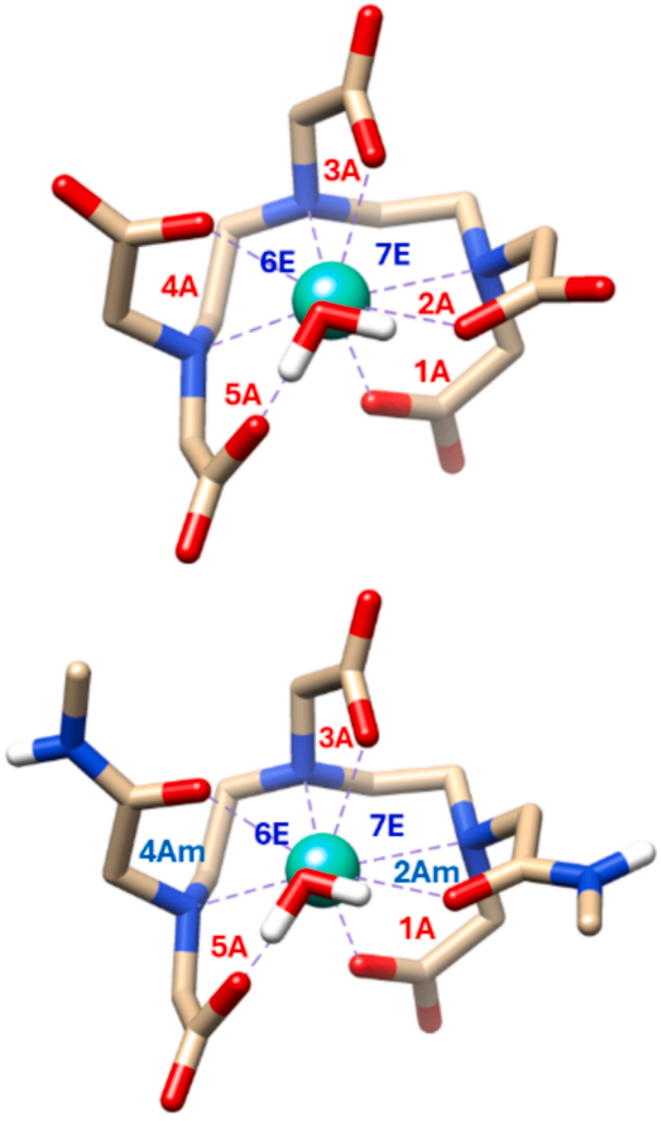

Fig. 5. Structures of the $[Gd(DTPA)(H_2O)]^{2-}$ (top) and $[Gd(DTPA\text{-}BMA)(H_2O)]$ (bottom) complexes obtained with DFT calculations and labelling of the five-membered chelate rings.

Table 2
Results of the fits of PESs of the $[Gd(DTPA)(H_2O)]^{2-}$ and $[Gd(DTPA\text{-}BMA)(H_2O)]$ complexes calculated with DFT.[a].

Chelate Ring	Donor group	k_{11} (×10^3 kcal mol^{-1} deg^{-2})	k_{111} (×10^5 kcal mol^{-1} deg^{-3})	k_{1111} (×10^7 kcal mol^{-1} deg^{-4})	ϕ_e (°)
1A	Acetate	2.71 ± 0.02	4.80 ± 0.04	3.33 ± 0.05	−26.5 ± 0.1
2A	Acetate	3.43 ± 0.02	0.31 ± 0.04	0.85 ± 0.08	–22.6 ± 0.1
2Am	Acetamide	3.79 ± 0.04	3.1 ± 0.1	[b]	−28.0 ± 0.2
3A	Acetate	3.10 ± 0.02	3.32 ± 0.05	3.42 ± 0.07	−20.9 ± 0.1
4A	Acetate	2.78 ± 0.02	4.43 ± 0.04	3.49 ± 0.05	–22.7 ± 0.1
4Am	Acetamide	3.40 ± 0.06	5.8 ± 0.1	3.2 ± 0.1	–23.3 ± 0.3
5A	Acetate	3.69 ± 0.02	1.9 ± 0.1	1.11 ± 0.04	–23.44 ± 0.06
6E	Ethylenediamine	19.5 ± 0.2	19.4 ± 0.4	[b]	65.0 ± 0.1
7E	Ethylenediamine	18.4 ± 0.1	17.2 ± 0.2	[b]	65.9 ± 0.1

[a] See Fig. 5 for labelling; standard errors of the least-squares fits are provided. [b] Value fixed to 0, as otherwise values with large statistical errors were obtained.

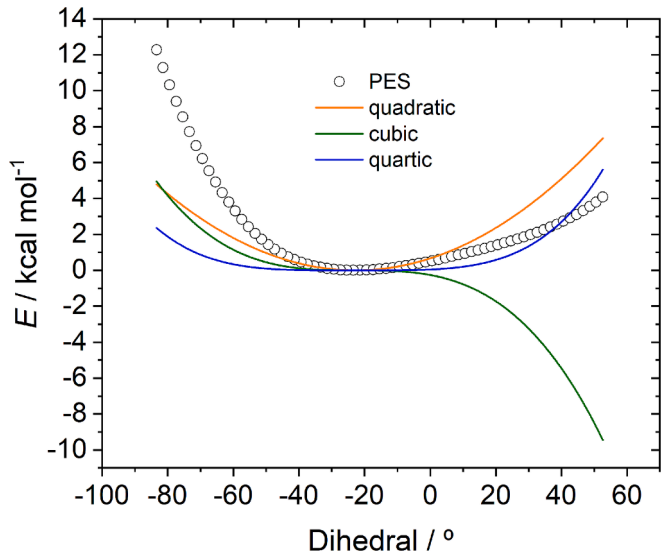

Fig. 6. Relaxed PESs obtained for acetate groups 4A in $[Gd(DTPA)(H_2O)]^{2-}$ and the contributions of quadratic, cubic and quartic terms of Eq [1] obtained from the fits of the data.

constants contribute to anharmonic shapes of the PESs.

The PESs of acetate and acetamide groups were investigated by comparing chelates 2A and 4A in $[Gd(DTPA)(H_2O)]^{2-}$ with the equivalent 2Am and 4Am chelates in $[Gd(DTPA\text{-}BMA)(H_2O)]$ (see Figs. 4 and 7). The optimised structure of $[Gd(DTPA\text{-}BMA)(H_2O)]$ displays a Λ(δδ) configuration, as observed in the solid state structures [75]. Thus, $[Gd(DTPA)(H_2O)]^{2-}$ and $[Gd(DTPA\text{-}BMA)(H_2O)]$ display very similar structures, which allows for a comparison of the five-membered chelate rings formed by acetate and acetamide groups. As a result, the PESs calculated for 2A/2Am and 4A/4Am have similar shapes. Inspection of the PESs indicates that acetamide groups provide deeper minima than the equivalent acetate groups, an effect that is reflected in the corresponding harmonic k_{111} force constants, which are significantly higher for acetamide groups compared to acetates (Table 2). This trend is again in good agreement with the narrower distribution of ϕ values observed in the solid state for acetamides compared to acetates. The effect is particularly evident for chelates 4A and 4Am, being less important for 2A and 2Am. The PESs calculated for the 2A/2Am and 4A/4Am pairs indicate that acetamide groups have somewhat higher cubic anharmonic contributions, as demonstrated by the corresponding k_{111} values. This indicates that the rotation of a methylacetamide group is less hindered by the environment compared with acetate groups, an effect that can be explained by the increasing electrostatic repulsion generated when two negatively charged carboxylate groups approach each other.

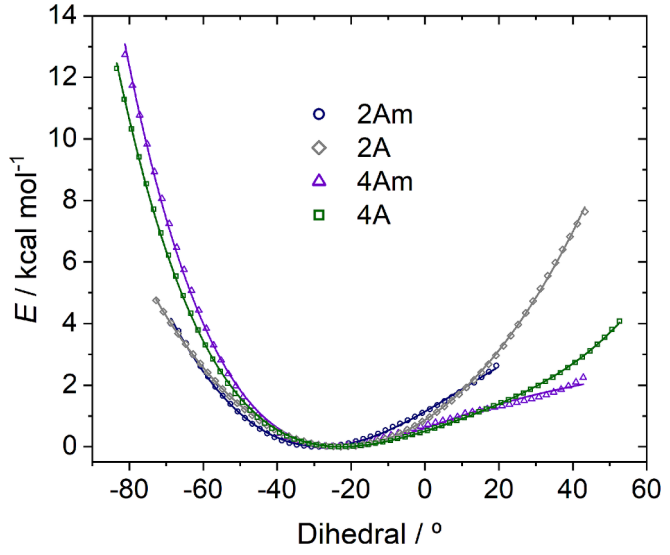

Fig. 7. Relaxed PESs obtained for acetate groups 2A and 4A in $[Gd(DTPA)(H_2O)]^{2-}$ compared with the 2Am and 4Am acetamide groups in $[Gd(DTPA\text{-}BMA)(H_2O)]$. The lines correspond to the fit of the data to Eq [1].

3.3. Other donor groups

A relatively large number of lanthanide complexes of DTPA and DOTA derivatives containing 2-methylpyridine or phosphinate groups were also characterized using X-ray diffraction. Given that the number of structures reported is more limited than for acetates and acetamides, we analysed the absolute angles of their N-C-C-N and N-C-P-O dihedrals (Fig. 8). The Gaussian distributions of pyridine and phosphinate groups are centered at 32.0 and 25.2°, respectively, with the pyridine donor being characterized by a narrow distribution (FWHM = 7.0°) and phosphinates showing a larger FWHM of 11.7°. The latter value is slightly lower than those characterizing acetamide groups (Table 1). Noteworthy, the mean N-C-C-N angle characterizing the dihedral angles of pyridine groups in TACN derivatives (35.3°, 119 values) is very similar to that observed for DTPA and DOTA complexes.

An additional set of DFT calculations was performed on the $[Gd(DOTA)(H_2O)]^{-}$, $[Gd(DOTAM)(H_2O)]^{3+}$, $[Gd(DOTP^{H})]^{-}$ and $[Gd(L^{PY})(H_2O)]^{3+}$ complexes, in order to compare the features of acetate, acetamide, phosphinate and pyridyl groups (Fig. 9). The X-ray structures of the four complexes were reported in the literature. The $[Gd(DOTA)(H_2O)]^{-}$ [76–78], $[Gd(DOTAM)(H_2O)]^{3+}$ [79–81] and $[Gd(L^{PY})(H_2O)]^{3+}$ [37] complexes display capped square antiprismatic coordination environments in the solid state, which correspond to the Λ(δδδδ)/Δ(λλλλ) enantiomeric pair [32,33]. On the other hand, the $[Gd(DOTP^{H})]^{-}$ complex displays a Δ(δδδδ)/Λ(λλλλ) configuration [82], which yields a twisted square antiprismatic coordination environment, as usually observed for DOTA derivatives containing bulky phosphonate or phosphinate arms [36].

The PESs calculated for these DOTA derivatives (Table 3) are similar to those calculated for the DTPA derivatives described above. The fits of the data afford k_{111} values that follow the trend acetate < acetamide < phosphinate < pyridine. This trend correlates very well with the linewidths of the Gaussian distributions obtained for these groups using X-ray data (Table 1), with a lower k_{111} value corresponding to a broader distribution. The bulky and negatively charged phosphinate group

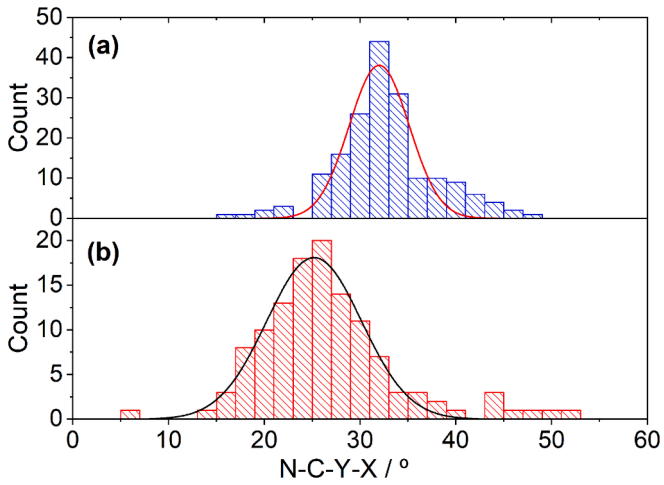

Fig. 8. Histograms showing the N-C-C-X dihedral angles characterizing five-membered chelate rings in DTPA and DOTA derivatives: (a) methylpyridine groups (X = N; Y = C); (b) methylphosphinate groups (X = O; Y = P). The solid lines correspond to the fits of the data to Gaussian distributions.

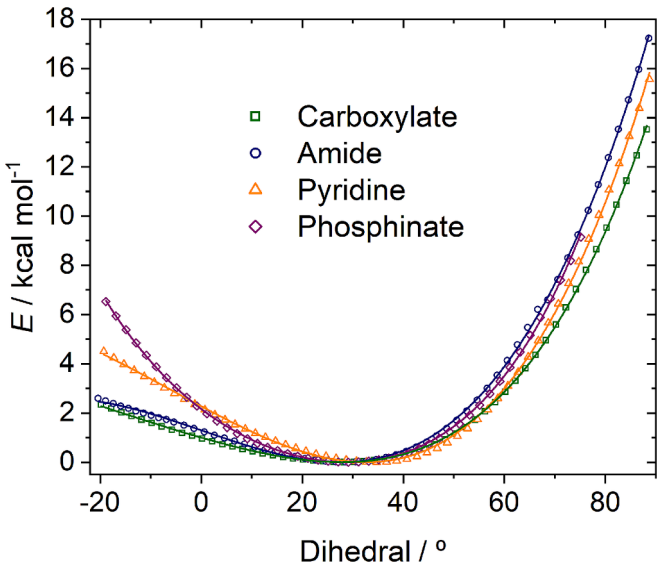

Fig. 9. Relaxed PESs obtained for the rotation of an acetate pendant arms in $[Gd(DOTA)(H_2O)]^-$, an acetamide arm in $[Gd(DOTAM)(H_2O)]^{3+}$, a pyridine arm in $[Gd(L^{PY})](H_2O)]^{3+}$ and a phosphinate arm in $[Gd(DOTPH)]^-$. The solid lines correspond to the fits of the data to Eq [1].

Table 3
Results of the fits of PESs of the $[Gd(DOTA)(H_2O)]^-$, $[Gd(DOTAM)(H_2O)]^{3+}$, $[Gd(DOTP^H)]^-$ and $[Gd(L^{PY})(H_2O)]^{3+}$ complexes calculated with DFT.[a].

Complex	Donor group	k_{11} ($\times 10^3$ kcal mol^{-1} deg^{-2})	k_{111} ($\times 10^5$ kcal mol^{-1} deg^{-3})	k_{1111} ($\times 10^7$ kcal mol^{-1} deg^{-3})	ϕ_e (°)
$[Gd(DOTA)(H_2O)]^-$	Acetate	3.71 ± 0.04	4.77 ± 0.08	2.5 ± 0.2	27.8 ± 0.2
$[Gd(DO3A)(H_2O)_2]^-$	Acetate	3.20 ± 0.01	4.12 ± 0.07	3.47 ± 0.06	26.2 ± 0.1
	Acetate	3.45 ± 0.02	5.19 ± 0.07	4.04 ± 0.07	28.1 ± 0.1
$[Gd(DOTAM)(H_2O)]^{3+}$	Acetamide	5.20 ± 0.07	6.5 ± 0.1	[b]	27.5 ± 0.2
$[Gd(DOTP^H)]^-$	Phosphinate	5.45 ± 0.05	3.2 ± 0.1	8.1 ± 0.3	28.8 ± 0.1
$[Gd(L^{PY})(H_2O)]^{3+}$	Pyridine	6.19 ± 0.08	6.3 ± 0.1	1.1 ± 0.3	32.2 ± 0.2

[a] Standard errors of the least-squares fits are provided. [b] Value fixed to 0, as otherwise values with large statistical errors were obtained.

exhibits the lowest k_{111} value among this series of complexes, indicating that environmental effects are playing an important role in hindering pendant arm rotation. The highest k_{111} values are obtained for the charge-neutral pendant arms, which suggests that electrostatic effects play a major role in this family of complexes containing four densely packed pendant arms.

A final set of calculations was performed on the $[Gd(DO3A)(H_2O)]$ complex to assess whether a less constrained structure will produce similar force constants. We thus analyzed the PESs of the terminal carboxylate groups, as one is lining towards the central acetate group and the second one towards a coordinated water molecule. These calculations provide rather similar PESs (Fig. S3, Supplementary material) and force constants (Table 3), with k_{11} values similar to those obtained for $[Gd(DOTA)(H_2O)]^-$, $[Gd(DTPA)(H_2O)]^{2-}$ and $[Gd(DTPA\text{-}BMA)(H_2O)]$, indicating that the quadratic force constants depend essentially on the nature of the donor group, while the cubic and quartic terms account for environmental effects.

The PESs calculated for carboxylate, amide, pyridine and phosphinate groups display a single minimum, in sharp constrast with the PES characterizing ethylenediamine groups (Fig. S4, Supplementary material). In the latter case, the PES reaches a maximum at around $\phi = 0$ in which the H atoms of the ethyl groups are eclipsed, leading to a second energy minimum. This process corresponds to a $\lambda \leftrightarrow \delta$ configurational change. This is in line with previous computational studies, which evidenced that the $(\lambda\lambda\lambda\lambda)\leftrightarrow(\delta\delta\delta\delta)$ interconversion is a stepwise process, each involving the inversion of an individual ethylenediamine group [34–37,83]. These results suggest that the arm rotation process in the complexes investigated here is likely to follow a concerted mechanism, involving simultaneous rotation of several donor groups. Concerted arm rotation processes were proposed for $[Ln(DOTA)]^-$ complexes using computational studies [34].

4. Conclusions

We have analysed the dihedral angles of different donor groups observed in the X-ray structures of lanthanide complexes with DOTA and DTPA derivatives. These torsion angles characterise the configuration of the corresponding five-membered chelate rings, either δ or λ, whose change in configuration are responsible for isomer interconversion in solution.

The analysis of the distribution of dihedral angles in the solid state, as well as the analysis of PESs with DFT, allows classifying the different five-membered chelate rings according to their resistance to deformation: acetate < acetamide < phosphinate < pyridine < ethylenediamine. This trend is consistently evidenced by both the FWHM of the Gaussian distributions obtained from X-ray data and the harmonic k_{11} force constants. The PESs characterising the $\lambda \leftrightarrow \delta$ configurational change of ethylenediamine units display two energy minima, suggesting that the isomer interconversion pathways involving the inversion of ethylenediamine units follow stepwise mechanisms. However, the PESs obtained for acetate, acetamide, phosphinate and pyridine groups are rather swallow and display a single energy minimum, suggesting that the isomer interconversion pathways involving $\lambda \leftrightarrow \delta$ configurational changes of these groups tend to follow concerted mechanisms. The harmonic k_{11} force constants for a given donor group fall within a rather narrow range, while the cubic and quartic force constants vary considerably due to environmental effects.

The results reported here have implications in ligand design, in particular if the goal is to obtain highly stable and inert complexes. In a recent work, we demonstrated that the thermodynamic stability of Gd(III) complexes can be predicted to a good accuracy by empirical expressions that consider the individual contribution of different groups [84]. However, the prediction of kinetic inertness is more challenging, as different pathways can lead to complex dissociation (i. e. spontaneous, proton assisted, metal assisted…) [16]. Nevertheless, complex rigidity has been identified as a key factor to attain kinetic inertness. The present contribution represents the first step towards quantifying the rigidity of metal complexes towards the prediction of the kinetic inertness of lanthanide complexes.

CRediT authorship contribution statement

Charlene Harriswangler: Writing – review & editing, Investigation, Data curation. **Saray Argibay-Otero:** Investigation, Data curation. **Antía Freire-García:** Investigation, Data curation. **M. Teresa Albelda:** Data curation. **Enrique García-España:** Funding acquisition, Data curation. **David Esteban-Gómez:** Methodology, Funding acquisition. **Juan C. Frías:** Writing – review & editing, Data curation, Conceptualization. **Carlos Platas-Iglesias:** Writing – original draft, Methodology, Funding acquisition, Formal analysis, Conceptualization.

Declaration of competing interest

The authors declare that they have no known competing financial

interests or personal relationships that could have appeared to influence the work reported in this paper.

Acknowledgements

Authors D.E.-G. and C.P.-I. thank Ministerio de Ciencia e Innovación (Grants PID2022-138335NB-I00 and RED2022-134091-T) and Xunta de Galicia (ED431C 2023/33) for generous financial support. C. H. and A. F.-G. thank Ministerio de Ciencia e Innovación (Grant PRE2020-092888) and Ministerio de Universidades (Grant FPU21/06305) for funding their PhD contracts. S. A.-O. thanks Ministerio de Universidades for funding her postdoctoral contract through the Margarita Salas program. E.G-E and M.T.A thanks Conselleria de Innovación, Universidades, Ciencia y Sociedad Digital of the Generalitat Valenciana (PROMETEO Grant CIPROM/2021/030). The authors thank Centro de Supercomputación de Galicia (CESGA) for providing the supercomputing facilities.

Appendix A. Supplementary data

Supplementary data to this article can be found online at https://doi.org/10.1016/j.inoche.2024.113348.

Data availability

Data will be made available on request.

References

[1] D. Parker, R.S. Dickins, H. Puschmann, C. Crossland, J.A.K. Howard, Being Excited by Lanthanide Coordination Complexes: Aqua Species, Chirality, Excited-State Chemistry, and Exchange Dynamics, Chem. Rev. 102 (2002) 1977–2010, https://doi.org/10.1021/cr010452+.
[2] V. Comblin, D. Gilsoul, M. Hermann, V. Humblet, V. Jacques, M. Mesbahi, C. Sauvage, J.F. Desreux, Designing new MRI contrast agents: a coordination chemistry challenge, Coord. Chem. Rev. 185–186 (1999) 451–470, https://doi.org/10.1016/S0010-8545(99)00028-4.
[3] J.-C.-G. Bünzli, Review: Lanthanide coordination chemistry: from old concepts to coordination polymers, J. Coord. Chem. 67 (2014) 3706–3733, https://doi.org/10.1080/00958972.2014.957201.
[4] K. Bernot, C. Daiguebonne, G. Calvez, Y. Suffren, O. Guillou, A Journey in Lanthanide Coordination Chemistry: From Evaporable Dimers to Magnetic Materials and Luminescent Devices, Acc. Chem. Res. 54 (2021) 427–440, https://doi.org/10.1021/acs.accounts.0c00684.
[5] X.-Z. Li, C.-B. Tian, Q.-F. Sun, Coordination-Directed Self-Assembly of Functional Polynuclear Lanthanide Supramolecular Architectures, Chem. Rev. 122 (2022) 6374–6458, https://doi.org/10.1021/acs.chemrev.1c00602.
[6] S.A. Cotton, P.R. Raithby, Systematics and surprises in lanthanide coordination chemistry, Coord. Chem. Rev. 340 (2017) 220–231, https://doi.org/10.1016/j.ccr.2017.01.011.
[7] T. Moeller, L.C. Thompson, Observations on the Rare Earths–LXXV. The Stabilities of Diethylenetriaminepentaacetic Acid Chelates, J. Inorg. Nucl. Chem. 24 (1962) 499–510.
[8] G. Anderegg, F. Arnaud-Neu, R. Delgado, J. Felcman, K. Popov, Critical Evaluation of Stability Constants of Metal Complexes of Complexones for Biomedical and Environmental Applications, Pure Appl. Chem. 77 (2005) 1445–1495, https://doi.org/10.1351/pac200577081445.
[9] G. Anderegg, CRITICAL SURVEY OF STABILITY CONSTANTS OF EDTA COMPLEXES, in: Crit. Surv. Stab. Constants EDTA Complexes, Elsevier, 1977: pp. 1–36. Doi: 10.1016/B978-0-08-022009-3.50004-0.
[10] J.F. Desreux, Nuclear magnetic resonance spectroscopy of lanthanide complexes with a tetraacetic tetraaza macrocycle. Unusual conformation properties, Inorg. Chem. 19 (1980) 1319–1324, https://doi.org/10.1021/ic50207a042.
[11] H.G. Brittain, J.F. Desreux, Luminescence and NMR studies of the conformational isomers of lanthanide complexes with an optically active polyaza polycarboxylic macrocycle, Inorg. Chem. 23 (1984) 4459–4466, https://doi.org/10.1021/ic00194a012.
[12] M.F. Loncin, J.F. Desreux, E. Merciny, Coordination of lanthanides by two polyamino polycarboxylic macrocycles: formation of highly stable lanthanide complexes, Inorg. Chem. 25 (1986) 2646–2648, https://doi.org/10.1021/ic00235a031.
[13] X. Wang, T. Jin, V. Comblin, A. Lopez-Mut, E. Merciny, J.F. Desreux, A kinetic investigation of the lanthanide DOTA chelates. Stability and rates of formation and of dissociation of a macrocyclic gadolinium(III) polyaza polycarboxylic MRI contrast agent, Inorg. Chem. 31 (1992) 1095–1099, https://doi.org/10.1021/ic00032a034.
[14] E. Tóth, E. Brücher, Stability constants of the lanthanide(III)-1,4,7,10-tetraazacyclododecane-N, N′, N″, N‴-tetraacetate complexes, Inorganica Chim. Acta 221 (1994) 165–167, https://doi.org/10.1016/0020-1693(94)03964-X.
[15] E. Toth, E. Brucher, I. Lazar, I. Toth, Kinetics of Formation and Dissociation of Lanthanide(III)-DOTA Complexes, Inorg. Chem. 33 (1994) 4070–4076, https://doi.org/10.1021/ic00096a036.
[16] Z. Baranyai, Z. Pálinkás, F. Uggeri, A. Maiocchi, S. Aime, E. Brücher, Dissociation Kinetics of Open-Chain and Macrocyclic Gadolinium(III)-Aminopolycarboxylate Complexes Related to Magnetic Resonance Imaging: Catalytic Effect of Endogenous Ligands, Chem. - Eur. J. 18 (2012) 16426–16435, https://doi.org/10.1002/chem.201202930.
[17] Z. Baranyai, E. Brücher, F. Uggeri, A. Maiocchi, I. Tóth, M. Andrási, A. Gáspár, L. Zékány, S. Aime, The Role of Equilibrium and Kinetic Properties in the Dissociation of Gd[DTPA-bis(methylamide)] (Omniscan) at near to Physiological Conditions, Chem. - Eur. J. 21 (2015) 4789–4799, https://doi.org/10.1002/chem.201405967.
[18] R.B. Lauffer, Paramagnetic metal complexes as water proton relaxation agents for NMR imaging: theory and design, Chem. Rev. 87 (1987) 901–927, https://doi.org/10.1021/cr00081a003.
[19] P. Caravan, J.J. Ellison, T.J. McMurry, R.B. Lauffer, Gadolinium(III) Chelates as MRI Contrast Agents: Structure, Dynamics, and Applications, Chem. Rev. 99 (1999) 2293–2352, https://doi.org/10.1021/cr980440x.
[20] J. Wahsner, E.M. Gale, A. Rodríguez-Rodríguez, P. Caravan, Chemistry of MRI Contrast Agents: Current Challenges and New Frontiers, Chem. Rev. 119 (2019) 957–1057, https://doi.org/10.1021/acs.chemrev.8b00363.
[21] J. Lohrke, M. Berger, T. Frenzel, C.-S. Hilger, G. Jost, O. Panknin, M. Bauser, W. Ebert, H. Pietsch, Preclinical Profile of Gadoquatrane: A Novel Tetrameric, Macrocyclic High Relaxivity Gadolinium-Based Contrast Agent, Invest. Radiol. 57 (2022) 629–638, https://doi.org/10.1097/RLI.0000000000000889.
[22] J.-C.-G. Bünzli, Lanthanide Luminescence for Biomedical Analyses and Imaging, Chem. Rev. 110 (2010) 2729–2755, https://doi.org/10.1021/cr900362e.
[23] J.-C.-G. Bünzli, On the design of highly luminescent lanthanide complexes, Coord. Chem. Rev. 293–294 (2015) 19–47, https://doi.org/10.1016/j.ccr.2014.10.013.
[24] M. Sy, A. Nonat, N. Hildebrandt, L.J. Charbonnière, Lanthanide-based luminescence biolabelling, Chem. Commun. 52 (2016) 5080–5095, https://doi.org/10.1039/C6CC00922K.
[25] A.M. Nonat, L.J. Charbonnière, Upconversion of light with molecular and supramolecular lanthanide complexes, Coord. Chem. Rev. 409 (2020) 213192, https://doi.org/10.1016/j.ccr.2020.213192.
[26] E.W. Price, C. Orvig, Matching chelators to radiometals for radiopharmaceuticals, Chem Soc Rev 43 (2014) 260–290, https://doi.org/10.1039/C3CS60304K.
[27] T.I. Kostelnik, C. Orvig, Radioactive Main Group and Rare Earth Metals for Imaging and Therapy, Chem. Rev. 119 (2019) 902–956, https://doi.org/10.1021/acs.chemrev.8b00294.
[28] U. Hennrich, M. Eder, [177Lu]Lu-PSMA-617 (PluvictoTM): The First FDA-Approved Radiotherapeutical for Treatment of Prostate Cancer, Pharmaceuticals 15 (2022) 1292, https://doi.org/10.3390/ph15101292.
[29] P. Caravan, D. Esteban-Gómez, A. Rodríguez-Rodríguez, C. Platas-Iglesias, Water exchange in lanthanide complexes for MRI applications. Lessons learned over the last 25 years, Dalton Trans. 48 (2019) 11161–11180, https://doi.org/10.1039/C9DT01948K.
[30] C.F.G.C. Geraldes, A.M. Urbano, M.A. Hoefnagel, J.A. Peters, Multinuclear magnetic resonance study of the structure and dynamics of lanthanide(III) complexes of the bis(propylamide) of diethylenetriaminepentaacetic acid in aqueous solution, Inorg. Chem. 32 (1993) 2426–2432, https://doi.org/10.1021/ic00063a037.
[31] S. Aime, M. Botta, G. Ermondi, NMR Study of Solution Structures and Dynamics of Lantbanide(III) Complexes of DOTA, Inorg. Chem. 31 (1992) 4291–4299, https://doi.org/10.1021/ic00047a016.
[32] S. Aime, M. Botta, M. Fasano, M.P.M. Marques, C.F.G.C. Geraldes, D. Pubanz, A. E. Merbach, Conformational and Coordination Equilibria on DOTA Complexes of Lanthanide Metal Ions in Aqueous Solution Studied by ^{1}H-NMR Spectroscopy, Inorg. Chem. 36 (1997) 2059–2068, https://doi.org/10.1021/ic961364o.
[33] C. Platas-Iglesias, The Solution Structure and Dynamics of MRI Probes Based on Lanthanide(III) DOTA as Investigated by DFT and NMR Spectroscopy, Eur. J. Inorg. Chem. 2012 (2012) 2023–2033, https://doi.org/10.1002/ejic.201101164.
[34] U. Cosentino, A. Villa, D. Pitea, G. Moro, V. Barone, A. Maiocchi, Conformational Characterization of Lanthanide(III)−DOTA Complexes by ab Initio Investigation in Vacuo and in Aqueous Solution, J. Am. Chem. Soc. 124 (2002) 4901–4909, https://doi.org/10.1021/ja017666t.
[35] J. Blahut, P. Hermann, Z. Tošner, C. Platas-Iglesias, A combined NMR and DFT study of conformational dynamics in lanthanide complexes of macrocyclic DOTA-like ligands, Phys Chem Chem Phys 19 (2017) 26662–26671, https://doi.org/10.1039/C7CP05296K.
[36] M. Purgel, Z. Baranyai, A. de Blas, T. Rodríguez-Blas, I. Bányai, C. Platas-Iglesias, I. Tóth, An NMR and DFT Investigation on the Conformational Properties of Lanthanide(III) 1,4,7,10-Tetraazacyclododecane-1,4,7,10-tetraacetate Analogues Containing Methylenephosphonate Pendant Arms, Inorg. Chem. 49 (2010) 4370–4382, https://doi.org/10.1021/ic100177n.
[37] L.S. Natrajan, N.M. Khoabane, B.L. Dadds, C.A. Muryn, R.G. Pritchard, S.L. Heath, A.M. Kenwright, I. Kuprov, S. Faulkner, Probing the Structure, Conformation, and Stereochemical Exchange in a Family of Lanthanide Complexes Derived from Tetrapyridyl-Appended Cyclen, Inorg. Chem. 49 (2010) 7700–7709, https://doi.org/10.1021/ic100447m.
[38] L. Tei, G. Gugliotta, D. Marchi, M. Cossi, S. Geninatti Crich, M. Botta, Optimizing the relaxivity at high fields: systematic variation of the rotational dynamics in

polynuclear Gd-complexes based on the AAZTA ligand, Inorg. Chem. Front. 8 (2021) 4806–4819, https://doi.org/10.1039/D1QI00904D.
[39] R. Puchta, N. van Eikema Hommes, R. Meier, R., van Eldik, A new enantiomerization mechanism for tripodal penta-coordinate ZnII(nta) complexes. Theoretical clarification of the observed 1H NMR spectrum, Dalton Trans. (2006) 3392, https://doi.org/10.1039/b602792j.
[40] F. Mayer, C. Platas-Iglesias, L. Helm, J.A. Peters, K. Djanashvili, ^{17}O NMR and Density Functional Theory Study of the Dynamics of the Carboxylate Groups in DOTA Complexes of Lanthanides in Aqueous Solution, Inorg. Chem. 51 (2012) 170–178, https://doi.org/10.1021/ic201393n.
[41] L. Fusaro, M. Luhmer, An oxygen-17 dynamic NMR study of the Pr–DOTA complex, Dalton Trans 43 (2014) 967–972, https://doi.org/10.1039/C3DT52533C.
[42] L. Fusaro, F. Mocci, R.N. Muller, M. Luhmer, Insight into the Dynamics of Lanthanide-DTPA Complexes As Revealed by Oxygen-17 NMR, Inorg. Chem. 51 (2012) 8455–8461, https://doi.org/10.1021/ic3010085.
[43] C. Harriswangler, J.C. Frías, M.T. Albelda, L. Valencia, E. García-España, D. Esteban-Gómez, C. Platas-Iglesias, Donor Radii in Rare-Earth Complexes, Inorg. Chem. 62 (2023) 17030–17040, https://doi.org/10.1021/acs.inorgchem.3c03126.
[44] T.R.M. Barends, L. Foucar, S. Botha, R.B. Doak, R.L. Shoeman, K. Nass, J.E. Koglin, G.J. Williams, S. Boutet, M. Messerschmidt, I. Schlichting, De novo protein crystal structure determination from X-ray free-electron laser data, Nature 505 (2014) 244–247, https://doi.org/10.1038/nature12773.
[45] M.J. Frisch, G.W. Trucks, H.B. Schlegel, G.E. Scuseria, M.A. Robb, J.R. Cheeseman, G. Scalmani, V. Barone, G.A. Petersson, H. Nakatsuji, X. Li, M. Caricato, A.V. Marenich, J. Bloino, B.G. Janesko, R. Gomperts, B. Mennucci, H.P. Hratchian, J.V. Ortiz, A.F. Izmaylov, J.L. Sonnenberg, Williams, F. Ding, F. Lipparini, F. Egidi, J. Goings, B. Peng, A. Petrone, T. Henderson, D. Ranasinghe, V.G. Zakrzewski, J. Gao, N. Rega, G. Zheng, W. Liang, M. Hada, M. Ehara, K. Toyota, R. Fukuda, J. Hasegawa, M. Ishida, T. Nakajima, Y. Honda, O. Kitao, H. Nakai, T. Vreven, K. Throssell, J.A. Montgomery Jr., J.E. Peralta, F. Ogliaro, M.J. Bearpark, J.J. Heyd, E.N. Brothers, K.N. Kudin, V.N. Staroverov, T.A. Keith, R. Kobayashi, J. Normand, K. Raghavachari, A.P. Rendell, J.C. Burant, S.S. Iyengar, J. Tomasi, M. Cossi, J.M. Millam, M. Klene, C. Adamo, R. Cammi, J.W. Ochterski, R.L. Martin, K. Morokuma, O. Farkas, J.B. Foresman, D.J. Fox, Gaussian 16 Rev. C.01, Wallingford, CT, 2016.
[46] J.-D. Chai, M. Head-Gordon, Systematic optimization of long-range corrected hybrid density functionals, J. Chem. Phys. 128 (2008) 084106, https://doi.org/10.1063/1.2834918.
[47] A. Nucera, C. Platas-Iglesias, F. Carniato, M. Botta, Effect of hydration equilibria on the relaxometric properties of Gd(iii) complexes: new insights into old systems, Dalton Trans. 52 (2023) 17229–17241, https://doi.org/10.1039/D3DT03413E.
[48] A. Roca-Sabio, M. Regueiro-Figueroa, D. Esteban-Gómez, A. de Blas, T. Rodríguez-Blas, C. Platas-Iglesias, Density functional dependence of molecular geometries in lanthanide(III) complexes relevant to bioanalytical and biomedical applications, Comput, Theor. Chem. 999 (2012) 93–104, https://doi.org/10.1016/j.comptc.2012.08.020.
[49] L. Leone, S. Camorali, A. Freire-García, C. Platas-Iglesias, D. Esteban Gomez, L. Tei, Scrutinising the role of intramolecular hydrogen bonding in water exchange dynamics of Gd(III) complexes, Dalton Trans. 50 (2021) 5506–5518, https://doi.org/10.1039/D1DT00204J.
[50] D. Esteban-Gómez, A. de Blas, T. Rodríguez-Blas, L. Helm, C. Platas-Iglesias, Hyperfine Coupling Constants on Inner-Sphere Water Molecules of Gd^{III} -Based MRI Contrast Agents, ChemPhysChem 13 (2012) 3640–3650, https://doi.org/10.1002/cphc.201200417.
[51] M. Regueiro-Figueroa, C. Platas-Iglesias, Toward the Prediction of Water Exchange Rates in Magnetic Resonance Imaging Contrast Agents: A Density Functional Theory Study, J. Phys. Chem. A 119 (2015) 6436–6445, https://doi.org/10.1021/acs.jpca.5b01728.
[52] M. Dolg, H. Stoll, A. Savin, H. Preuss, Energy-adjusted pseudopotentials for the rare earth elements, Theor. Chim. Acta 75 (1989) 173–194, https://doi.org/10.1007/BF00528565.
[53] J. Yang, M. Dolg, Valence basis sets for lanthanide 4f-in-core pseudopotentials adapted for crystal orbital ab initio calculations, Theor. Chem. Acc. 113 (2005) 212–224, https://doi.org/10.1007/s00214-005-0629-0.
[54] F. Weigend, R. Ahlrichs, Balanced basis sets of split valence, triple zeta valence and quadruple zeta valence quality for H to Rn: Design and assessment of accuracy, Phys. Chem. Chem. Phys. 7 (2005) 3297–3305, https://doi.org/10.1039/b508541a.
[55] J. Tomasi, B. Mennucci, E. Cancès, The IEF version of the PCM solvation method: an overview of a new method addressed to study molecular solutes at the QM ab initio level, J. Mol. Struct. THEOCHEM 464 (1999) 211–226, https://doi.org/10.1016/S0166-1280(98)00553-3.
[56] J. Tomasi, B. Mennucci, R. Cammi, Quantum Mechanical Continuum Solvation Models, Chem. Rev. 105 (2005) 2999–3094, https://doi.org/10.1021/cr9904009.
[57] G.D. Purvis, R.J. Bartlett, A full coupled-cluster singles and doubles model: The inclusion of disconnected triples, J. Chem. Phys. 76 (1982) 1910–1918, https://doi.org/10.1063/1.443164.
[58] M. Dolg, H. Stoll, H. Preuss, Energy-adjusted *ab inio* pseudopotentials for the rare earth elements, J. Chem. Phys. 90 (1989) 1730–1734, https://doi.org/10.1063/1.456066.
[59] M. Bazargan, M. Mirzaei, A. Franconetti, A. Frontera, On the preferences of five-membered chelate rings in coordination chemistry: insights from the Cambridge Structural Database and theoretical calculations, Dalton Trans. 48 (2019) 5476–5490, https://doi.org/10.1039/C9DT00542K.
[60] A. Ehnbom, S.K. Ghosh, K.G. Lewis, J.A. Gladysz, Octahedral Werner complexes with substituted ethylenediamine ligands: a stereochemical primer for a historic series of compounds now emerging as a modern family of catalysts, Chem. Soc. Rev. 45 (2016) 6799–6811, https://doi.org/10.1039/C6CS00604C.
[61] B.G. Jenkins, R.B. Lauffer, Solution structure and dynamics of lanthanide(III) complexes of diethylenetriaminepentaacetate: a two-dimensional NMR analysis, Inorg. Chem. 27 (1988) 4730–4738, https://doi.org/10.1021/ic00299a011.
[62] N. Hamon, A. Roux, M. Beyler, J.-C. Mulatier, C. Andraud, C. Nguyen, M. Maynadier, N. Bettache, A. Duperray, A. Grichine, S. Brasselet, M. Gary-Bobo, O. Maury, R. Tripier, Pyclen-Based Ln(III) Complexes as Highly Luminescent Bioprobes for *In Vitro* and *In Vivo* One- and Two-Photon Bioimaging Applications, J. Am. Chem. Soc. 142 (2020) 10184–10197, https://doi.org/10.1021/jacs.0c03496.
[63] A.M. Funk, K.-L.-N.-A. Finney, P. Harvey, A.M. Kenwright, E.R. Neil, N.J. Rogers, P. Kanthi Senanayake, D. Parker, Critical analysis of the limitations of Bleaney's theory of magnetic anisotropy in paramagnetic lanthanide coordination complexes, Chem. Sci. 6 (2015) 1655–1662, https://doi.org/10.1039/C4SC03429E.
[64] L. Valencia, J. Martinez, A. Macías, R. Bastida, R.A. Carvalho, C.F.G.C. Geraldes, X-ray Diffraction and ^{1}H NMR in Solution: Structural Determination of Lanthanide Complexes of a $Py_2N_6Ac_4$ Ligand, Inorg. Chem. 41 (2002) 5300–5312, https://doi.org/10.1021/ic0257017.
[65] T. Gambino, L. Valencia, P. Pérez-Lourido, D. Esteban-Gómez, M. Zaiss, C. Platas-Iglesias, G. Angelovski, Inert macrocyclic Eu^{3+} complex with affirmative paraCEST features, Inorg. Chem. Front. 7 (2020) 2274–2286, https://doi.org/10.1039/C9QI01612K.
[66] M. Regueiro-Figueroa, D. Esteban-Gómez, A. de Blas, T. Rodríguez-Blas, C. Platas-Iglesias, Structure and Dynamics of Lanthanide(III) Complexes with an N-Alkylated do3a Ligand (H_3do3a = 1,4,7,10-Tetraazacyclododecane-1,4,7-triacetic Acid): A Combined Experimental and DFT Study, Eur. J. Inorg. Chem. 2010 (2010) 3586–3595, https://doi.org/10.1002/ejic.201000334.
[67] S. Aime, A. Barge, A. Borel, M. Botta, S. Chemerisov, A.E. Merbach, U. Müller, D. Pubanz, A Multinuclear NMR Study on the Structure and Dynamics of Lanthanide(III) Complexes of the Poly(amino carboxylate) $EGTA^{4-}$ in Aqueous Solution, Inorg. Chem. 36 (1997) 5104–5112, https://doi.org/10.1021/ic970240o.
[68] R. Negri, Z. Baranyai, L. Tei, G.B. Giovenzana, C. Platas-Iglesias, A.C. Bényei, J. Bodnár, A. Vágner, M. Botta, Lower Denticity Leading to Higher Stability: Structural and Solution Studies of Ln(III)–OBETA Complexes, Inorg. Chem. 53 (2014) 12499–12511, https://doi.org/10.1021/ic5020225.
[69] Z. Baranyai, D. Delli Castelli, C. Platas-Iglesias, D. Esteban-Gomez, A. Bényei, L. Tei, M. Botta, Combined NMR, DFT and X-ray studies highlight structural and hydration changes of $[Ln(AAZTA)]^-$ complexes across the series, Inorg. Chem. Front. 7 (2020) 795–803, https://doi.org/10.1039/C9QI01442J.
[70] L.G. Nielsen, H.O.B. Andersen, A.M. Kenwright, C. Platas-Iglesias, T.J. Sørensen, Using chiral auxiliaries to mimic the effect of chiral media on the structure of lanthanide(III) complexes common in bioimaging and diagnostic MRI, Inorg. Chem. 63 (2024) 7560–7570, https://doi.org/10.1021/acs.inorgchem.3c01589.
[71] R. Janicki, A. Mondry, Structural and thermodynamic aspects of hydration of Gd (iii) systems, Dalton Trans. 48 (2019) 3380–3391, https://doi.org/10.1039/C8DT04869J.
[72] S. Gao, S.J. George, Z.-H. Zhou, Interaction of Gd-DTPA with phosphate and phosphite: toward the reaction intermediate in nephrogenic systemic fibrosis, Dalton Trans. 45 (2016) 5388–5394, https://doi.org/10.1039/C5DT04172D.
[73] B. Zhao, X.-Y. Chen, W.-Z. Wang, P. Cheng, B. Ding, D.-Z. Liao, S.-P. Yan, Z.-H. Jiang, {[GdAg2(dtpa)(H2O)]·3H2O}n: the first 2D Gd–Ag coordination polymer with Ag–Ag interaction, Inorg. Chem. Commun. 8 (2005) 178–181, https://doi.org/10.1016/j.inoche.2004.12.004.
[74] D.G. Truhlar, Potential Energy Surfaces, in: Encycl. Phys. Sci. Technol., 3rd ed., Academic Press, New York, 2001: pp. 9–17. Doi: 10.1016/B0-12-227410-5/00606-2.
[75] A. Aukrust, T. Engebretsen, L.K. Sydnes, L.J. Sæthre, K.W.T. And, Hydrates of Gadolinium Diethylenetriaminepentaacetic Acid Bis(methylamide) as Studied by X-ray Diffraction, Org. Process Res. Dev. 5 (2001) 361–367, https://doi.org/10.1021/op000106e.
[76] P. Thuéry, The first uranyl–lanthanide heterometallic complexes: metal–organic frameworks with DOTA and oxalato ligands, CrystEngComm 10 (2008) 1126, https://doi.org/10.1039/b808611g.
[77] C.A. Chang, L.C. Francesconi, M.F. Malley, K. Kumar, J.Z. Gougoutas, M. F. Tweedle, D.W. Lee, L.J. Wilson, Synthesis, characterization, and crystal structures of M(DO3A) (M = iron, gadolinium) and Na[M(DOTA)] (M = Fe, yttrium, Gd), Inorg. Chem. 32 (1993) 3501–3508, https://doi.org/10.1021/ic00068a020.
[78] P. Thuéry, Structural variability in uranyl–lanthanide heterometallic complexes with DOTA and oxalato ligands, CrystEngComm 11 (2009) 2319, https://doi.org/10.1039/b907392b.
[79] A. Barge, M. Botta, D. Parker, H. Puschmann, The nature of the counter-anion can determine the rate of water exchange in a metal aqua complexElectronic supplementary information (ESI) available: representative NMRD profile (298 K) and 17O-NMR analysis for the chloride complex. See http://www.rsc.org/suppdata/cc/b3/b302211k/, Chem. Commun. (2003) 1386–1387. Doi: 10.1039/b302211k.
[80] G. Bombieri, N. Marchini, S. Ciattini, A. Mortillaro, S. Aime, The crystallized solvent could influence the lanthanide water bonding? Inorganica Chim. Acta 359 (2006) 3405–3411, https://doi.org/10.1016/j.ica.2006.03.023.
[81] A.L. Thompson, D. Parker, D.A. Fulton, J.A.K. Howard, S.U. Pandya, H. Puschmann, K. Senanayake, P.A. Stenson, A. Badari, M. Botta, S. Avedano, S. Aime, On the role of the counter-ion in defining water structure and dynamics:

order, structure and dynamics in hydrophilic and hydrophobic gadolinium salt complexes, Dalton Trans. (2006) 5605–5616, https://doi.org/10.1039/b606206g.
[82] Z. Kotková, G.A. Pereira, K. Djanashvili, J. Kotek, J. Rudovský, P. Hermann, L. Vander Elst, R.N. Muller, C.F.G.C. Geraldes, I. Lukeš, J.A. Peters, Lanthanide(III), complexes of phosphorus acid analogues of H_4DOTA as model compounds for the evaluation of the second-sphere hydration, Eur. J. Inorg. Chem. 2009 (2009) 119–136, https://doi.org/10.1002/ejic.200800859.
[83] M. Regueiro-Figueroa, B. Bensenane, E. Ruscsák, D. Esteban-Gómez, L. J. Charbonnière, G. Tircsó, I. Tóth, A. de Blas, T. Rodríguez-Blas, C. Platas-Iglesias, Lanthanide dota-like complexes containing a picolinate pendant: structural entry for the design of Ln^{III} -based luminescent Probes, Inorg. Chem. 50 (2011) 4125–4141, https://doi.org/10.1021/ic2001915.
[84] R. Uzal-Varela, A. Rodríguez-Rodríguez, H. Wang, D. Esteban-Gómez, I. Brandariz, E.M. Gale, P. Caravan, C. Platas-Iglesias, Prediction of Gd(III) complex thermodynamic stability, Coord. Chem. Rev. 467 (2022) 214606, https://doi.org/10.1016/j.ccr.2022.214606.